ERK2-topoisomerase II regulatory axis is important for gene activation in immediate early genes

Authors:

Deukyeong Kim[1], Masahiro Naganuma[2], Reiko Nakagawa[3], Anh Cong[4], Haruhiko Ehara[2], Hongha Vu[5], Jaehyeon Jeong[6], Jeong Ho Chang[5], Matthew J. Schellenberg[4], Shun-ichi Sekine[2] and Heeyoun Bunch[1,6]*

Affiliations:

[1]School of Applied Biosciences, College of Agriculture & Life Sciences, Kyungpook National University, Daegu 41566, Republic of Korea

[2]Laboratory for Transcription Structural Biology, RIKEN Center for Biosystems Dynamics Research, 1-7-22 Suehiro-cho, Tsurumi-ku, Yokohama 230-0045, Japan

[3]RIKEN BDR Laboratory for Phyloinformatics, Hyogo 650-0047, Japan

[4]Department of Biochemistry and Molecular Biology, Mayo Clinic, Rochester, MN 55905, USA

[5]Department of Biology Education, Kyungpook National University, Daegu 41566, Republic of Korea

[6]Department of Applied Biosciences, Kyungpook National University, Daegu 41566, Republic of Korea

*Correspondence to HB at heeyounbunch@gmail.com

ABSTRACT

Transcription of stress-inducible genes requires synchronized and robust activation, which is critical for organismal survival and homeostasis. The function of mitogen-activated protein kinase (MAPK) signaling pathway is involved in the activation of immediate early genes (IEGs), including *EGR1* and *FOS*, for cell growth[1-3]. In addition, recent studies have identified topoisomerase II (TOP2) as one of the important regulators of the transcriptional activation in IEGs[4-6]. However, the mechanism underlying transcriptional regulation involving TOP2 in IEG activation remains unknown. Here, we demonstrate that ERK2, but not ERK1, is important for IEG transcriptional activation and report a critical ELK1 binding sequence for ERK2 function at the *EGR1* gene. Our data indicated that both ERK1 and ERK2 extensively phosphorylate the C-terminal domain of TOP2B at mutual and

distinctive residues. Inhibition of ERK2 kinase activity or ERK2 knock-down interferes with transcription and deregulates TOP2B in IEGs. Furthermore, the cryo-EM structure of the TOP2B-*EGR1* transcription start site-etoposide complex demonstrated breakage and dramatic bending of the double-stranded DNA, suggesting the mechanism of TOP2B-mediated transcriptional activation. Taken together, this study suggests that the activated ERK2 phosphorylates TOP2B to regulate TOP2-DNA interactions during transcriptional activation in IEGs. We propose that TOP2B association, catalysis, and dissociation on its substrate DNA are important for regulating transcription and that ERK2-mediated TOP2B phosphorylation may be important for the dissociation step.

Keywords:
Transcriptional regulation; ERK2; *EGR1*; immediate early genes; RNA polymerase II pause release; topoisomerase II regulation; topoisomerase IIβ; gene activation

INTRODUCTION

Transcription is the first step in gene expression, where RNA is synthesized by a DNA-dependent RNA polymerase. In eukaryotic cells, RNA polymerase II (Pol II) is the core enzyme for the transcription of protein-coding mRNA and some non-protein coding RNA[7]. Pol II routinely synthesizes mRNAs in house-keeping genes, whereas its activity is timely and tightly regulated by transcriptional activators and repressors in inducible genes. In particular, stress-inducible genes respond to environmental signals and cellular needs, and their synchronized and rapid gene expression is crucial for cell survival, maintenance, and growth[2,5,8-10]. Representative examples are serum/growth factor-inducible immediate early genes (IEGs)[2,5], heat shock genes[11-13], neurotransmitter-inducible genes[4,14], enhancer RNA genes[15,16], and hypoxia-inducible genes[17,18].

Recent studies have identified key mechanisms of these stress-inducible genes in metazoan cells. To ensure synchronized and rapid transcriptional onset, Pol II is paused at the transcription start site (TSS) during the early elongation, between transcriptional initiation and productive elongation[10,19]. Pol II promoter-proximal pausing (Pol II pausing hereafter) is caused by multiple elements, namely, protein factors, nucleic acid sequences and structures, and chromatin architecture[20-25]. Likewise, the release of Pol II pausing involves the collaborations of such elements as transcriptional activators,

structural/topological changes of DNA, and modifications of chromatin dynamics[4,5,12,24,26-29]. For example, heat shock and serum induction activate transcriptional activators, HSF1 and MAP kinases such as ERK1 and ERK2, respectively[12,30,31]. While HSF1 is the sole master activator that binds to target gene promoters to induce transcriptional activation[32,33], ERK1 and ERK2 require upstream kinases and downstream substrates, which are gene-specific, nuclear DNA binding transcriptional activators, such as FOS and ELK, to activate their target genes[34,35]. Previous studies showed that Pol II pausing at heat shock and IEGs is reversed by the binding of these gene specific transcriptional activators[5,24,27,36]. Simultaneous with the activator binding to its target gene promoter, the catalytic function of TOP2 is required for Pol II pause release[4,5,28,37-39]. Furthermore, transcriptional activation triggers and requires DNA damage response (DDR) signaling which is reduced when TOP2 is inhibited by ICRF193, a catalytic inhibitor of TOP2[5]. This finding suggests that the topological alteration of DNA by TOP2 is important for Pol II pause release. Consistently, other studies have reported that DNA breaks are abundant in Pol II pausing sites[40], that TOP2 covalent cleavage complex is frequently formed in estrogen-induced transcription[41,42], and that both positive and negative supercoiling of DNA could inhibit Pol II forward-translocation[43,44]. These suggest that the DNA at Pol II pausing sites requires the catalytic function of TOP2 and is susceptible to DNA damage.

Human TOP2 proteins, including the two isomers TOP2A and TOP2B, resolve topological stresses during DNA metabolisms such as replication, transcription, and chromosomal compaction[45-47]. TOP2 catalyzes both positive and negative supercoiling as well as decatenation[45]. Previously, TOP2A was considered to be involved in replication while TOP2B in transcription[5,37,46,48]. However, recent studies have suggested that both TOP2A and TOP2B are important regulators of stress-inducible gene transcription[4-6,37,39,49]. Moreover, most conventional TOP2 chemical inhibitors, including ICRF193 and etoposide, target both enzymes, making it difficult to distinguish their effects on TOP2A and TOP2B[50]. TOP2A and TOP2B share 67% homology at the protein level, which is largely distinctive in the C-terminal domain (CTD)[51]. In the complex of 20–30 nt double stranded DNA, the cryo-electron microscopy (cryo-EM) structure of a full-length human TOP2A was recently reported, whereas only a partial human TOP2B (445–1201 aa) lacking both terminal domains could be resolved by crystallography[52-54]. In the study, the CTD (1191–1531 aa) of TOP2A protein was unstructured and could not be arrayed either by 2D or 3D reconstruction[52]. However, the biochemical analyses with

mutant TOP2A lacking the CTD suggested that the CTD allosterically regulates the catalytic activity of the enzyme[52].

Over 200 protein-coding genes can be simultaneously turned on within minutes of serum/growth factor induction. Some of these genes are potent transcription factors that activate the expression of a large number of genes for cell cycle progression[5,55,56]. Representative such IEGs include *EGR1*, *FOS*, *JUN*, and *MYC*[5,56]. ERK1 and ERK2 proteins are key MAP kinases that activate these genes by phosphorylating the downstream DNA-binding transcriptional activators including ELK1, FOS, and MYC[2,57]. *EGR1* and *FOS* gene expression is also reportedly activated by ERKs and ELK1[56,57]. ERK1 and ERK2 proteins are approximately 82.6% identical, with their distinctive N-terminal sequences. While some studies have suggested redundant functions of ERK1 and ERK2, others have reported differential and opposite functions of ERK1 and ERK2[58-62]. Furthermore, ERK2-mediated phosphorylation of TOP2A was reported[63], suggesting potential functional interactions between ERK proteins and TOP2.

In this study, we attempted to understand transcriptional regulation in IEGs by ERK1 and ERK2 proteins and investigated their interaction with TOP2B. Biochemical, structural, and cell-based analyses revealed the differential functions of ERK1 and ERK2 in IEG transcription and demonstrated that human TOP2B is extensively phosphorylated by both ERK1 and ERK2. However, ERK2, but not ERK1, activates transcription. The catalytic inhibition or knock-down (KD) of ERK2 caused an abnormal increase of TOP2B at the representative IEGs. In addition, we present the cryo-EM structure of the human TOP2B DNA binding/catalytic domain in a ternary complex with a 50 nt segment of *EGR1* TSS and etoposide, suggesting a mechanism of TOP2B-mediated transcriptional activation.

MATERIALS & METHODS

Cell culture and conditions. Cell culture and serum induction of HEK293 were carried out as previously described[5,6,64]. For TOP2B inhibitors, ICRF193 (Sigma, I4659) and etoposide (Sigma, 341205) were used at a final concentration of 10 μM in 0.1% DMSO for 3 h. An ERK2 inhibitor, VX-11e (Selleck, S7709) was used at a final concentration of 100 nM in 0.1% DMSO for 3–5 h. Control

cells were treated with the same amount of DMSO for the same duration. Serum starvation and induction were performed as previously described[5,6].

Cell transfection and knock-down experiment. HEK293 cells were grown to 60–70% confluence in a complete medium. The medium was replaced with Opti-MEM (Gibco, 31985) before transfecting with scrambled siRNA (Santa Cruz Biotechnology, sc-37007) and ERK1 siRNA (Cell Signaling Technology, #6436), ERK2 siRNA (Santa Cruz Biotechnology, sc-35335), or both ERK siRNA species. Lipofectamine 2000 (Invitrogen) or FuGENE HD (Promega, E2311) transfection reagent was used according to the manufacturer's instructions. The transfected cells were collected after 48 h or 72 h incubation for RNA or protein/ChIP analyses, respectively. HEK293 cell extracts were prepared using a RIPA buffer (Cell Signaling Technology) in the presence of freshly added protease inhibitors (1 mM benzamidine, 0.25 mM PMSF, 1 mM Na-metabisulfite, 1 mM DTT; chemicals purchased from Sigma). Protein concentrations in the cell extracts were determined by Bradford assays (Bio-Rad Laboratories) using BSA standard curves.

Real-time PCR. Total RNA was purified using the RNeasy kit (Qiagen) following the manufacturer's instructions. The concentration of RNA was measured using Nanodrop and 0.6 μg of purified RNA was converted into cDNA by reverse transcription using ReverTra Ace qPCR RT Master Mix (Toyobo). Real-time PCR was conducted with equal amounts of resultant cDNAs, the indicated primers (Table S1), and SYBR Green PCR Master Mix (Applied Biosystems) using the StepOnePlus Real-Time PCR System (Applied Biosystems). β-Actin was used as the normalizer. Thermal cycles were as follows: 1 min at 95°C followed by 45 cycles of 15 s at 95°C , 15 s at 55°C, and 1 min at 72 °C. The results are presented as relative fold differences, standard deviations (SDs), and statistical validations (see below).

DNA template construction. The *EGR1* template DNA, –423 to +332, was cloned into a pCR-Blunt-TOPO to generate pTOPO-EGR1[6]. The biotinylated *EGR1* template was PCR-amplified using a pair of primers, one conjugated with biotin at the 5' end (Table S1), and prepared using the same method described in our previous study[6]. ELK1m was constructed using a set of primers (Table S1), introducing the desired mutation, and pTOPO-EGR1 as a template. The resultant ELK1m construct

was sequenced for validation. All primers used in this study were purchased from Integrated DNA Technology.

HeLa NE and protein preparation. HeLa nuclei were provided by Dr. D. J. Taatjes at the University of Colorado. HeLa NE was prepared as previously described[6,24]. WT and mutant ERK1 (human) and ERK2 (mouse) bacterial expression vectors were generated from a previous study[65] and gifted by Drs. N. Soudah and D. Engelberg at the Hebrew University of Jerusalem. To express human ERK2, we incorporated two amino acids and a point mutation, which are the only differences between human and mouse ERK2 proteins, into the WT and mutant ERK2 plasmids using two pairs of primers (Table S1). BL21 cells were grown in Luria-Bertani (LB) medium (Qmbrothia) containing 50 mg/L kanamycin (Applichem). The expression of recombinant ERK protein was induced by 0.3 mM isopropyl-β-D-thiogalactopyranoside (IPTG) at an optical density of 0.6. Cells were further incubated at 20 °C for 18h. Cells were harvested, resuspended in the binding buffer (50 mM Tris pH 8.0, 150 mM NaCl, 5 mM β-mercaptoethanol) and lysed by ultrasonication (SONICS, VCX-500/750), followed by cell debris removal by centrifugation. The supernatant was collected and loaded onto a Ni-NTA HiTrap chelating column (GE Healthcare). After eluting the bound proteins with an elution buffer containing 500 mM imidazole (50 mM Tris pH 8.0, 150 mM NaCl, 5 mM β-mercaptoethanol, 500 mM imidazole), the target protein was further purified using a HiPrep 16/60 Sephacryl S-300 HR column (GE Healthcare). The size-exclusion column buffer contained 50 mM Tris pH 7.5, 150 mM NaCl, 1 mM dithiothreitol (DTT). Human full-length TOP2B was purified from HEK cells, as previously described[6,66]. For the *in vitro* kinase assay, mass spectrometry, and cryo-EM, ubiquitin-stripped TOP2B[6] was used. The activity of purified TOP2B was confirmed using an *in vitro* decatenation assay, as previously described[6]. Full-length ELK1 gene was amplified from pCGN-ELK1 purchased from Addgene (plasmid #27156) using a set of primers (Table S1) including XhoI and NdeI (New England Biolabs) and KOD plus NEO polymerase (Toyobo). The ELK1 PCR product was digested with the above restriction endonucleases and ligated to the pET17b plasmid, which was linearized with the same enzymes, using T4 DNA ligase (New England Biolabs). The cloned ELK1 was validated by sequencing (Macrogen). *E. coli* BL21 strain was transformed with the resultant plasmid, pET17b-ELK1. The bacterial cells were grown to OD_{600} 0.3–0.4 and ELK1 protein expression was induced at 30°C for 5 h using 0.2 mM IPTG. The cells were lysed with the xTractor Bacterial Cell Lysis Buffer (Clontech) and sonicated. His^6-tagged ELK1 was purified on a Ni affinity column using

the same method as previously described[6,24]. The purified proteins were validated by SDS-PAGE and immunoblotting (see the antibody information below).

Immobilized template assay and Immunoblotting. The procedure and reagents for the immobilized template assay were identical to those used in our previous studies[6,24]. Dynabeads M-280 Streptavidin (Invitrogen) was washed and equilibriated with 2× B&W buffer (10 mM Tris-HCl, pH 7.5, 1 mM EDTA, 2 M NaCl) and incubated with biotin-conjugated *EGR1* template DNA (–423 to +332) at 10 ng DNA/μL beads. The template-conjugated beads were washed twice with 1× B&W buffer and twice with 0.1 M Buffer D1 (20 mM HEPES, pH 7.6, 20% glycerol, 0.1 mM EDTA, 100 mM KCl). For each reaction, 120 ng of immobilized template was resuspended in NE buffer (17.5 ng/μL dI–dC, 0.1% NP40, 7.5 mM $MgCl_2$, 1.25 μg/μL BSA, 8.7% glycerol, 8.7 mM HEPES, pH 7.6, 44 μM EDTA, 130 mM KCl, 10 μM $ZnCl_2$). HeLa NE and purified recombinant WT or mutant ERK proteins at 100 μg/reaction, when indicated, were incubated with agitation for 30 min at room temperature (RT) to assemble the PIC. The template-protein complex was washed with a 10 beads volume of TW buffer (13 mM HEPES, pH 7.6, 13% glycerol, 60 mM KCl, 7 mM $MgCl_2$, 7 mM DTT, 100 μM EDTA, 0.0125% NP40, 10 μM $ZnCl_2$) and then the beads were resuspended in TC buffer I (13 mM HEPES, pH 7.6, 13% glycerol, 60 mM KCl, 7 mM $MgCl_2$, 10 μM $ZnCl_2$, 7 mM DTT, 100 μM EDTA, 15 ng/μL dI-dC, 10 mM creatine phosphate) for *in vitro* transcription assay (see below) or in SDS-loading buffer for protein quantification using SDS-PAGE and immunoblotting. TF, NE, TW, and TC buffers were supplemented with freshly added protease, 1 mM benzamidine, 0.25 mM PMSF, 1 mM Na-metabisulfite, 1 mM DTT, and aprotinin (Sigma A6279, 1:1000). The primary antibodies used in this study were Pol II (ab817, Abcam; #2629, Cell Signaling Technology; A304-405A, Bethyl Laboratories), CDK9 (sc-13130, Santa Cruz Biotechnology), MED23 (A300-425A, Bethyl Laboratories), ELK1 (sc-365876, Santa Cruz Biotechnology; #91825, Cell Signaling Technology), ERK1/2 (ab17942, Abcam), and TOP2B (A300-949A, Bethyl Laboratories; sc-25330, Santa Cruz Biotechnology).

***In vitro* transcription and RNA quantification.** For *in vitro* transcription assay, the procedure and reagents were identical as previously described[6,24], except for the method used to quantify the *in vitro* synthesized *EGR1* mRNA molecules. A mixture of NTP at a final concentration of 250 μM A/G/C/U was added to the reactions prepared using the immobilized template assay. The mixture was

incubated at 30 °C for 30 min to allow Pol II to polymerize mRNA molecules. When ERK proteins were assayed, the purified proteins were included during the PIC assembly and after 3–5 min of NTP addition. The polymerization reaction was proceeded for 30 min. Subsequently, 1.5 Kunitz unit DNase I (Qiagen) was added to the reaction and allowed to sit for an additional 15 min to digest the template DNA. The reaction was terminated with five volumes of 1.2× Stop buffer (0.6 M Tris-HCl, pH 8.0, 12 mM EDTA, 100 μg/mL tRNA). The pellet fraction, including the magnetic beads and the supernatant, was separated using a magnetic stand (Invitrogen). The supernatant was treated with an equal volume of phenol: chloroform: isoamyl alcohol (25:24:1, Sigma) solution to extract proteins. The soluble fraction, including RNA, was precipitated with 2.6 volumes of 100% ethanol (Sigma). Following centrifugation at 14,000 rpm for 30 min, the pellet was dissolved in nuclease-free water. The RNA was incubated at 70 °C for 10 min, followed by centrifugation at 10,000 rpm for 1 min. The cDNA construction mixture included 5 mM $MgCl_2$, 10× buffer, 1 mM dNTP mixture, AMV reverse transcriptase, random primers, and RNA, according to the manufacturer's instructions (Promega). The PCR conditions were 25 °C for 10 min, 42 °C for 60 min, and 95 °C for 5 min. The resulting cDNA was quantified using SYBR Green (Applied Biosystems) and real-time quantitative PCR (Applied Biosystems), using a primer set for probing *EGR1* mRNA (Table S1).

Cryo-EM sample preparation and image processing. Double-stranded DNA was produced by annealing of two complementary DNA strands: 5′-GAGTCGCGAGAGATCCCAGCGCGCAGAACTTGGGGAGCCGCCGCCGCCAT-3′ and 5′-ATGGCGGCGGCGGCTCCCCAAGTTCTGCGCGCTGGGATCTCTCGCGACTC-3′ (Integrated DNA Technology). For the TOP2B-DNA-etoposide complex formation, 8.3 μM TOP2B, 16.7 μM dsDNA, and 1.67 μM etoposide were mixed in a buffer containing 20 mM HEPES pH 8.0, 5 mM KCl, 5 mM $MgCl_2$, and 0.5 mM ATP. Quantifoil grids (R1.2/1.3, Cu, 300 mesh; Quantifoil Micro Tools) were glow-discharged for 1.5 min using a PIB-10 ION Bombarder (Vacuum Device Inc.) immediately before use. Two microliters of sample were applied to the glow-discharged grids, which were blotted for 3 s and plunge-frozen in liquid ethane using a Vitrobot Mark IV (FEI) operated at 4 °C and 100% humidity (blotforce 5; blottime 3).

Cryo-EM data collection and image processing. Micrographs were acquired on a Krios G4 transmission electron microscope (ThermoFisher Scientific) with a K3 detector and a BioQuantum

energy filter (Gatan) operated with a slit width of 15 eV. Data collection was automated using EPU software and micrographs were taken at a magnification of 105,000× (0.83 Å per pixel) with a total dose of 49 e/A2, fractionated over 40 frames. A total of 2327 micrographs were acquired. Estimation of the contrast-transfer function was performed with Gctf[67]. Motion correction, 2D and 3D classification steps, and further processing were performed using RELION 3.0[68]. Particle picking was done by using Warp[69] and Topaz[70], and those particles were merged while avoiding overlap. Particles were first extracted with 3x binning (2.49 Å/pixel), and junk particles were removed using a series of 2D and 3D classifications. The remaining particles were re-extracted with a pixel size of 1.245 Å/pixel, and then refined with masks around TOP2B. Bayesian polishing and CTF refinement were then applied. Masks were created using the UCSF Chimera[71]. During 3D refinement, C2-symmetry was imposed.

Model building and refinement. The refined map was used for model building. For the TOP2B-DNA-etoposide complex structure, we first docked the existing structural models into the density. We used the TOP2B model deposited in the AlphaFold Protein Structure Database (Uniprot code: Q02880) as an initial TOP2B model. For the initial models of dsDNA and etoposide, we used the crystal structure of the TOP2B-DNA-etoposide complex, deposited in the Protein Data Bank (PDB code: 3QX3). As the nucleotide sequence could not be identified in the density map, the DNA model ws tentatively built in that the middle of the DNA sequence was placed in the middle of the TOP2B DNA binding domain. The model was fitted into the refined map in UCSF Chimera[71] and manually edited in Coot[72], followed by real-space refinement with PHENIX[73], using secondary structures and base-pairing restrains. The final models were validated in Molprobity[74] and the figures were generated using UCSF Chimera and PyMol (Schrödinger LLC).

Chromatin immunoprecipitation and qPCR. ChIP-qPCR analysis was conducted following the previously described methods and reagents without modifications[5,6,24]. The antibodies used for this study were phosphorylated S2 Pol II (ab5095, Abcam) and TOP2B (A300-949A, Bethyl Laboratories). The primer sets used are listed in Table S1.

***In vitro* kinase assay.** The substrate, 1.8 μg of TOP2B was incubated with approximately 0.5 μg WT or mutant ERK proteins as a kinase in a reaction. For the control reaction, TOP2B without any kinase

was prepared side-by-side. Kinase buffer included 25 mM Tris pH 8.0, 2 mM DTT, 500 μM cold ATP, 100 mM KCl, 10 mM $MgCl_2$, and 2.5 μCi γ-P^{32} (PerkinElmer) labeled ATP to be final concentrations per a reaction. The reaction was incubated at 30 °C for 3.5 h before it was terminated using an 8× SDS-loading buffer. One microliter of each reaction was run on a 7% SDS-PAGE gel and visualized by silver-staining (silver nitrate, Sigma). The rest of the reaction was subjected to SDS-PAGE followed by autoradiography. For mass spectrometry, only cold ATP without γ-P^{32} labeled ATP was used and separated on a 7% SDS-PAGE gel. The bands corresponding to TOP2B were meticulously sliced for the further analysis.

Mass spectrometry. Proteins in each gel slice were extracted using in-gel digestion. The gel slices were diced into 1 mm pieces, and subjected to reduction with 10 mM Tris (2-carboxyethyl) phosphine hydrochloride (Sigma) at 56°C for 1 h, alkylated with 55 mM iodoacetamide at RT for 45 min in the dark, and digested with 500 ng of trypsin (Thermo Scientific) at 37°C for 16 h. The resulting peptides were extracted using 1% trifluoroacetic acid and 50% acetonitrile. Phosphorylated peptides were enriched using the High-Select Fe-NTA Phosphopeptide Enrichment Kit (Thermo Scientific) following the manufacturer's instructions. The enriched fractions were desalted with an in-house-made C18 stage-tip. Mass spectra were obtained on an LTQ-Orbitrap Velos Pro (Thermo Scientific) coupled with a nanoflow UHPLC system (ADVANCE UHPLC, AMR Inc.) and Advanced Captive Spray SOURCE (AMR Inc.). The peptides mixtures were fractionated using C18 reverse-phase chromatography (3 μm, ID 0.075 mm × 150 mm, CERI). The peptides were eluted at a flow rate of 300 nL/min with a linear gradient of 5–35% solvent B over 60 min. The compositions of solutions A and B were 2% acetonitrile and 0.1% formic acid and 100% acetonitrile, respectively. The mass spectrometer was programmed to carry out seven successive scans, with the first consisting of a full MS scan from 350–1600 m/z using Orbitrap (resolution = 60 K). The second to fourth was data-dependent scans of the top three abundant ions obtained in the first scan using an ion trap with CID. The fifth to seventh was data-dependent scans of the top three abundant ions obtained in the first scan using Orbitrap(resolution = 7,500) with HCD. Automatic MS/MS spectra were obtained from the highest peak in each scan by setting the relative collision energy to 35% CID or HCD and the exclusion time to 90 s for molecules in the same m/z value range. The raw files were searched against the Uniprot Human proteome database (2020.2.26 downloaded) and cRAP contaminant protein dataset using the MASCOT program (version 2.6; Matrix Science) via Proteome Discoverer 2.4 (Thermo Fisher

Scientific). The search was performed using carbamidomethylation of cysteine as a fixed modification, oxidation of methionine, acetylation of protein N-termini, and phosphorylation of serine, threonine, and tyrosine as variable modifications. The number of missed cleavages sites was set as 2.

Statistical analysis. Standard deviation was calculated and used to generate error bars. The Student's t-test was used to determine statistical significance ($P < 0.05$). Graphs were generated using the Prism 8 software (GraphPad, Inc.).

RESULTS

ERK2, but not ERK1, activates *EGR1* transcription

We investigated the function of ERK1 and ERK2 in IEG transcription using *EGR1* as a model gene. Previously, the *EGR1* template DNA including –432 to +332 was constructed and validated for *in vitro* biochemical analyses[6]. A schematic representation of the immobilized template assay is presented in **Fig. 1A**. The biotinylated *EGR1* template was conjugated with the avidin-coated magnetic beads. The HeLa nuclear extract (NE) was used to assemble the preinitiation complex on the DNA in the presence of competitor oligomers. Recombinant ERK1 or ERK2 purified from bacteria were included along with NE (**Fig. 1B**; K1 for ERK1 and K2 for ERK2). Following incubation, unbound or loosely bound proteins were washed off. The proteins of interest that were stably associated with the template were detected using immunoblotting (**Fig. 1A**). ERK1 and ERK2 supplemented reactions were compared with a buffer-only control (none) for their ability to recruit signature factors that are important for transcriptional activation, namely, Pol II, CDK9 (a catalytic subunit of P-TEFb), and MED23 (a subunit of the Mediator complex)(**Fig. 1C**). Interestingly, only ERK2 consistently and notably increased all three factors, whereas ERK1 did not (**Fig. 1C**; **Supplementary Fig. 1A**).

We believed that the effect of ERK1 and ERK2 could be compromised since the protein source of HeLa NE used for the immobilized template assay included mostly nuclear proteins, lacking the upstream, cytosolic components of the MAPK pathway to activate them[2,57]. Therefore, constitutively active recombinant ERK1 and ERK2 mutants, R84S and R67S[65], respectively, were purified from

bacteria (**Fig. 1D**; ERK1 mutant as K1m/ERK1m and ERK2 mutant as K2m/ERK2m). Immobilized template assays using these proteins, comparing WT and mutant ERKs, indicated that ERK2 and ERK2m were more proficient in recruiting Pol II, MED23, and CDK9 than ERK1 and ERK1m (**Fig. 1E**; **Supplementary Fig. 1B**). Immobilized template assays followed by *in vitro* transcription assays consistently demonstrated that ERK2 and ERK2m activated the *EGR1* transcription (**Fig. 1F**). In contrast, ERK1 and ERK1m repressed transcription (**Fig. 1F**), suggesting the opposite regulatory effects of ERK1 and ERK2 on *EGR1* transcription.

ERK2-mediated transcriptional activation requires ELK1 at the *EGR1* gene

Next, we investigated whether ERK2-mediated *EGR1* gene activation was dependent on a DNA-binding transcription factor ELK1. A previous study reported the consensus ELK1 binding sequence (CCGGAAGT) in human breast epithelial MCF10A cells using ChIP-seq[75] (**Fig. 2A**). The *EGR1* promoter (–423 to –1) includes numerous sites with over 75% homology to this ELK1 consensus sequence although only one site (GCTTCCGG, –338 to –345) has over 85% homology (87.5%; **Fig. 2A**). Therefore, we hypothesized that it may be a critical ELK1 binding site to mutate this region to TAAATTAA in the immobilized *EGR1* template DNA (ELK1^{m}; **Fig. 2A**). The immobilized template assay comparing the WT and ELK1^{m} indicated that ELK1 binding was markedly reduced in the ELK1^{m} *EGR1* template (**Figs. 2B**,**C**). In addition, TOP2B and CDK9 recruitment were significantly reduced on the template (**Figs. 2B**,**C**; **Supplementary Fig. 1B**). We tested the transcriptional activity of WT, ERK1m, and ERK2m proteins on the WT and ELK1^{m} templates, using the immobilized template assay. The results demonstrated that Pol II and MED23 recruitment by ERK2 and ERK2m on the WT template was abolished to the background level on the ELK1^{m} template (**Fig. 2D**; **Supplementary Fig. 1B**). These data were consistent with those from the *in vitro* transcription assays, showing that the ERK2-mediated transcriptional activation was strongly suppressed on the ELK1^{m} template (**Fig. 2E**). Collectively, the mutated segment, –338 to –345, appeared to be important for both ELK1 binding and ERK2 transactivation at *EGR1*, *in vitro* (**Figs. 1C–F**, **2D**).

ERK1 and ERK2 phosphorylate TOP2B on mutual and distinctive sites

We noted that TOP2B association with the *EGR1* TSS was positively correlated with ELK1 binding (**Figs. 2B**,**C**; **Supplementary Fig. 1B**). In addition, it has been previously shown that TOP2B is recruited to IEGs, including the *EGR1* gene, upon transcriptional activation[5,6]. Moreover, TOP2B

inhibition using ICRF193 suppresses Pol II pause release and productive transcription in these genes[5]. Therefore, we attempted to understand the relationship between transcriptional activation and TOP2B at the *EGR1* gene. The results indicated that both ERK1m and ERK2m enhanced the recruitment of TOP2B to the *EGR1* TSS in the immobilized template assay (**Fig. 3A**; **Supplementary Fig. 1B**). However, ERK2m was more effective in recruiting TOP2B (**Fig. 3A**; **Supplementary Fig. 1B**). Both ERK1m and ERK2m failed to recruit TOP2B to the ELK1^{m} template (**Fig. 3A**; **Supplementary Fig. 1B**), suggesting that ERK-mediated TOP2B enrichment could be ELK1-dependent.

We hypothesized that ERKs might recruit and phosphorylate TOP2B. This appears plausible as it was reported previously that TOP2A is phosphorylated by ERK2 *in vitro*[63]. To verify this hypothesis, *in vitro* kinase assays with human TOP2B (180 KDa) purified from human HEK cells and WT and mutant ERKs proteins were performed. Purified TOP2B and ERKs proteins used in the assays were silver-stained and are shown in **Figs. 1B**, **1D**, **3B**, and **3C**. Recombinant ELK1 (47 KDa) purified from *E. coli* was used as a positive control for ERKs (**Fig. 3C**; **Supplementary Fig. 2A**). After the kinase assay, a portion of each reaction was visualized by SDS-PAGE, followed by silver-staining (**Fig. 3C**), and analyzed by autoradiography (**Fig. 3D**; **Supplementary Fig. 2B**). As expected, the control, ELK1 was phosphorylated by both ERK1 and ERK2 (**Fig. 3D**). Although the intensity was milder, ERK1 and ERK2 phosphorylated TOP2B (**Fig. 3D**). In contrast, TOP2B was intensively phosphorylated by the constitutively active ERKs, ERK1m and ERK2m (**Fig. 3D**; **Supplementary Fig. 2B**).

Interestingly, TOP2B was phosphorylated by both ERK1 and ERK2 (**Fig. 3D**) although ERK1 and ERK2 showed differential effects on *EGR1* transcription (**Figs. 1C–F**). Thus, it is essential to understand if there are any differences in ERK1- vs ERK2-mediated TOP2B phosphorylation that allows these proteins to affect TOP2B differentially. To address this question, TOP2B was phosphorylated by ERK1m and ERK2m *in vitro* and was sliced out from the gel after separation by SDS-PAGE (**Fig. 3E**). A negative control, HEK cell-purified TOP2B itself without *in vitro* phosphorylation, was included (mock, **Fig. 3E**). The trypsin-digested phosphopeptides of TOP2B were enriched and analyzed using mass spectrometry (**Figs. 3E**,**F**). In the assay, coverages for TOP2B peptides ($p < 0.05$) in the control and phosphorylated samples were 50–70% (**Supplementary Data 1–3**). We observed that some residues were already phosphorylated in the

control. These residues were excluded from data collection. Our results indicated that ERK1m and ERK2m phosphorylated both mutual and distinctive residues on TOP2B (**Fig. 3G**). Notably, most of ERK-mediated phospho-sites were mapped to the CTD of TOP2B. In particular, four ERK2-specific phospho-sites (S1342, T1403, S1473, S1588) were exclusively concentrated in the CTD (**Fig. 3G**).

Cryo-EM structure of the TOP2B-*EGR1* TSS-etoposide complex

To understand the function of TOP2B CTD phosphorylation by ERK2 in *EGR1* transcription, we attempted to map these phospho-sites in the 3D structure. Thus, the cryo-EM structure of a full-length TOP2B-EGR1 TSS complex (50 bp, from –30 to +20) was obtained. The protein-DNA complex itself was unstable but could be stabilized by the addition of etoposide, a small chemical inhibitor that traps TOP2 in the TOP2-DNA cleavage complex, which is otherwise a transient intermediate. The cryo-EM structure of the ternary complex was determined at a nominal resolution of 3.9 Å (**Fig. 4A; Supplementary Data 4**). A density map was obtained by performing 2D and 3D classifications and 3D refinement (**Supplementary Fig. 3A–D**; **Table S2**). The density of the ATPase domain of TOP2B (1–456 aa) was observed in the 2D and 3D reconstructions (**Supplementary Fig. 3D–F)**. However, interpretable maps in 3D refinement were not obtained probably because of its intrinsic flexibility relative to the core domain. We observed that two TOP2B molecules (DNA binding and catalytic core domains: 457–1118 aa and 1140–1207 aa) formed a symmetric dimer (**Fig. 4A–C**; **Supplementary Fig. 3E**). The overall structure was comparable to the TOP2B crystal structure reported previously[54]. The CTD (1208–1626 aa) was disordered and could not be determined; therefore, we were unable to map the ERK2-phosphorylated residues on TOP2B. However, we learned that the DNA was dramatically bent by approximately 90° and bound to the cavity formed by the TOP2B dimer when complexed with *EGR1* TSS and etoposide (**Figs. 4A**–**C**). Both of the two DNA strands were cleaved at the active site of each TOP2B (**Fig. 4B**). Two etoposide molecules were intercalated into the two cleavage sites of the double strand of *EGR1* TSS. When HEK293 cells were treated with 10 μM etoposide for 3 h, *EGR1* transcription was significantly increased (**Fig. 4D**). However, ICRF193, a small catalytic inhibitor of TOP2, decreased the transcription (**Fig. 4D**), as previously shown[5]. These results, together with the cryo-EM structure, strongly suggest that the DNA cleavage and bending caused by TOP2B positively regulate transcriptional activation of the *EGR1* gene.

ERK2-mediated phosphorylation of TOP2B regulates TOP2B release at the *EGR1* gene

We sought to understand the function of ERK2-mediated phosphorylation of TOP2B during transcriptional activation via inhibition of the catalytic activity of ERK2. VX-11e (VX11) is a small chemical inhibitor, specific to ERK2[76,77]. HEK293 cells were treated with 100 nM VX11 for 3 h. The *EGR1* mRNA expression was measured by reverse transcription followed by real-time quantitative PCR (qRT-PCR). The results indicated that VX11 effectively reduced *EGR1* transcription (**Fig. 5A**). *HSP70*, a control gene that is not an ERK2 target gene, was not affected by these conditions (**Fig. 5A**). The inhibitory effect of VX11 was more dramatic when *EGR1* was transcriptionally activated by serum induction for 15 min (DMSO/S15 vs. VX11/S15) after synchronizing the cell cycle at G0 by serum starvation (DMSO/S0, VX11/S0)(**Fig. 5B**). Similar results were shown for the transcription of the *FOS* gene, another IEG and ERK2-target gene, that VX11 treatment interfered with *FOS* mRNA synthesis (**Fig. 5B**). Moreover, S2 Pol II occupancy at *EGR1* was notably reduced in the VX11/S15 samples, compared with the DMSO/S15 control (**Fig. 5C**). TOP2B in the *EGR1* TSS became increased upon serum induction (DMSO/S0 vs DMSO/S15, **Fig. 5D**), as it was previously demonstrated that TOP2B is recruited upon transcriptional activation in IEGs. Strikingly, VX11 treatment markedly increased TOP2B occupancy even in the transcriptional resting state (VX11/S0), to a degree much higher than that of the DMSO control. Serum induction in the presence of VX11 further increased *EGR1* TSS-bound TOP2B (**Fig. 5D**).

Since we hypothesized that transcriptional repression by VX11 might counteract the recruitment of TOP2B in transcriptional activation, the increased TOP2B occupancies with VX11 treatment were surprising and required further validation. Thus, we downregulated ERK2 and quantitatively measured the occupancy of TOP2B associated with the *EGR1* TSS. ERK KD using small interfering RNA species targeting ERK1 ($K1^{KD}$), ERK2 ($K2^{KD}$), or both proteins ($Double^{KD}$) was performed in HEK293 cells. Immunoblotting confirmed a reduction in targeted proteins (**Fig. 5E**). qRT-PCR and ChIP-qPCR data comparing these cells indicated that ERK2 KD decreased *EGR1* mRNA production and dramatically increased TOP2B occupancy with the *EGR1* TSS, respectively (**Fig. 5F**). On the other hand, ERK1 or double KD did not affect the *EGR1* expression. Double KD did not affect TOP2B occupancy in the *EGR1* TSS (**Fig. 5F**). Similar results were obtained for the *FOS* gene: only ERK2 KD decreased the gene expression and increased TOP2B association (**Fig. 5G**). Collectively, the results from ERK2 catalytic inhibition by VX11 and KD experiments suggest that the absence of functional ERK2 results in abnormal TOP2B accumulation, repressing transcription at *EGR1* gene.

DISCUSSION

ERK1 and ERK2 are considered to have redundant roles,[59,62] although some studies have reported their different, even opposite functions in certain biological pathways, such as cell proliferation[58,60,61,78,79]. Some studies have investigated the foundation of these differences between ERK1 and ERK2 proteins. For example, ERK1 and ERK2 have dramatically different trafficking or shuffling rates from the cytosol to the nucleus, which is due to the less conserved N-terminal domains between these two proteins[80]. In another previous study, an N-terminal deletion mutant (Δ19–25) functioned as a dominant negative mutant for the endogenous ERK2[81], suggesting the importance of the N-terminal region for the unique nature of ERK2. In this study, we examined ERK1 and ERK2 and presented their distinct roles in IEG transcriptional activation. The results suggest that ERK2 activates *EGR1* transcription (**Figs. 1C**,**F**,**5F**; **Supplementary Fig. 1**), which provides the mechanistic explanation for previous observations of the ERK2 role in cell proliferation[58,60,78]. It is unclear whether the N-terminal domains of ERK1 and ERK2 contribute to their distinctive roles in the transcriptional activation of IEGs. It will be important to understand the differential and mutual functions, interactomes, and dynamics of ERK1 and ERK2 in the future.

ERK1 and ERK2 are the key kinases in the MAPK pathway that promote cell growth. ELK1 and MYC are among the targets of ERK1 and ERK2[34,57,75]. Studies have suggested an interaction between ERK1/ERK2 and TOP2[63,82]. While a study showed that ERK2 phosphorylates and activates TOP2A, it also identified that a diphosphorylated catalytic mutant version of ERK2 still activates TOP2A[63], suggesting that the interaction between phosphorylated ERK2 and TOP2A, not TOP2A phosphorylation by ERK2, is required for TOP2A activation. In another study, TOP2 poisoning increased ERK1/2 phosphorylation and ERK1/2 inhibition reduces TOP2 poisoning-induced cell cycle arrest[82]. In this study, we showed that TOP2B is a substrate of ERK1 and ERK2 (**Fig. 3**; **Supplementary Data 1–3**). Interestingly, a few sites are mutually phosphorylated by both the kinases, whereas four residues uniquely phosphorylated by ERK2 are located in the TOP2B CTD (**Fig. 3G**). Since ERK2 catalytic inhibition using VX11 caused a dramatic increase in TOP2B occupancies in the *EGR1* TSS (**Fig. 5D**), it is suggested that the lack of ERK2-dependent phosphorylation of TOP2B at these sites may account for this unusual accumulation of TOP2B.

Consistently, ERK2 KD, but not ERK1 or double KD, increased TOP2B in the TSSs of *EGR1* and *FOS* genes (**Figs. 5F**,**G**). It is unclear what is the role of the accumulated TOP2B, an important question to be answered in future. Perhaps, these are the TOP2B molecules that might be either abnormally recruited or trapped (unable to be released from) on the DNA. TOP2B recruitment and catalysis of DNA double-strand breaks typically occur in the TSS of IEGs, leading to IEG activation (**Figs. 3A, 5B**)[4,5]. However, in the case of ERK2 catalytic inhibition and KD, IEG expression was hindered (**Figs. 5A–C**, **5E–G**), suggesting that TOP2B is not activated to catalyze the DNA but stays on the DNA in the absence of functional ERK2. This is supported by the observations that ICRF193, which causes TOP2B to be stuck on DNA without catalysis[83,84], inhibits transcription at *EGR1* and other IEGs (**Fig. 4D**)[5].

In contrast to ICRF193, etoposide treatment induced gene activation in *EGR*1 and *FOS* (**Fig. 4D**). In the structural data obtained, the *EGR1* TSS associated with the core TOP2B domain and etoposide exhibited a dramatic bending of DNA, approximately 90°, each DNA strand cleaved by a TOP2B protein (**Figs. 4A–C**). The bending of the TSS could bring the promoter and the TSS, where Pol II is paused in stimulus-inducible genes, to a proximity. This allows DNA-binding transcriptional activators in the promoter to interact with the paused Pol II in the TSS to reverse pausing and activate transcription. DNA bending is believed to play a positive role in transcriptional activation[85-88]; however, the exact roles of DNA break and DDR in transcription are not well understood. Although topological stresses during transcription require the function of TOP1 and TOP2[4-6,28,29,37], TOP2-mediated DNA catalysis does not typically result in DDR[28]. In spite of the dogma, transcription is coupled with DDR signaling and the activation of DNA repair enzymes, and the catalytic function of TOP2B contributes to transcription and DDR activation[4-6,24,28]. Thus, it is likely that DDR signaling is activated when TOP2B is removed from the broken site without rejoining it to expose the lesion. To the best of our knowledge, it is not clear whether DNA break and DDR are byproducts of transcriptional activation or play an active role in it. However, it should be noted that inhibiting DDR or critical DNA repair enzymes interferes with Pol II pause release and gene expression[4-6,17,24,89], suggesting a proactive role of DNA break and DDR in transcriptional activation. Moreover, it is not difficult to find the examples of purposed and functional DNA fragmentation and small nucleic acid production in DNA metabolisms such as DNA replication[90], recombination[91], and repair[92]. In the

future, it will be important to understand the role of TOP2-mediated DNA break and the mechanisms of TOP2 regulation for gene activation.

Acknowledgments

We are grateful to D. Engelberg and N. Soudah at the Hebrew University of Jerusalem for their generosity in sharing the bacterial WT and mutant ERK1/2 expression vectors and to D.J. Taatjes at the University of Colorado for the gift of HeLa NE. We thank S. Lee, D. Kim, M. Seu, and the current members of the Bunch laboratory members at Kyungpook National University (KNU) for their technical assistance. H.B. thanks D.Y. Bunch, John, and J. Christ for their loving encouragement and support throughout the course of this work.

Financial Supports

This research was supported by grants from the Japan Society for the Promotion of Science (KAKENHI, JP20H05690) to S.S. and from the National Research Foundation (NRF) of the Republic of Korea (2022R1A21003569) to H.B.

Author Contributions

DK and HB performed the immobilized template and transcription assays and mass spectrometry sample preparation. DK carried out quantitative real-time PCR of ChIP and RNA analyses and immunoblotting. MN, HE, and SS performed cryo-EM data collection and structure determination: the cryo-EM experiments were performed at the RIKEN Yokohama cryo-EM facility. RN performed mass spectrometry. AC, MS, HV, and JC performed the protein purification. DK and JJ performed cloning, mutagenesis, and SDS-PAGE. HB performed the kinase assay, cell culture, drug treatment, KD experiments, ChIP, and immunoblotting. HB created the hypothesis, designed the experiments, analyzed and curated the data, and wrote and revised the manuscript.

Declaration of Interests

The authors declare that they have no competing interests.

Data and Materials Availability

All data are available in the manuscript or as supplementary information. The cryo-EM map and coordinates were deposited to the Electron Microscopy Database (EMDB) and to the PDB under the following accession codes: EMD-34022 and PDB 7YQ8.

References

1. Murphy, L.O., MacKeigan, J.P. & Blenis, J. A network of immediate early gene products propagates subtle differences in mitogen-activated protein kinase signal amplitude and duration. *Mol Cell Biol* **24**, 144-53 (2004).
2. Whitmarsh, A.J., Shore, P., Sharrocks, A.D. & Davis, R.J. Integration of MAP kinase signal transduction pathways at the serum response element. *Science* **269**, 403-7 (1995).
3. Yue, J. et al. Integrator orchestrates RAS/ERK1/2 signaling transcriptional programs. *Genes Dev* **31**, 1809-1820 (2017).
4. Madabhushi, R. et al. Activity-Induced DNA Breaks Govern the Expression of Neuronal Early-Response Genes. *Cell* **161**, 1592-605 (2015).
5. Bunch, H. et al. Transcriptional elongation requires DNA break-induced signalling. *Nat Commun* **6**, 10191 (2015).
6. Bunch, H. et al. BRCA1-BARD1 regulates transcription through modulating topoisomerase IIbeta. *Open Biol* **11**, 210221 (2021).
7. Eidem, T.M., Kugel, J.F. & Goodrich, J.A. Noncoding RNAs: Regulators of the Mammalian Transcription Machinery. *J Mol Biol* **428**, 2652-2659 (2016).
8. Pakos-Zebrucka, K. et al. The integrated stress response. *EMBO Rep* **17**, 1374-1395 (2016).
9. Bunch, H. Role of genome guardian proteins in transcriptional elongation. *FEBS Lett* **590**, 1064-75 (2016).
10. Jonkers, I. & Lis, J.T. Getting up to speed with transcription elongation by RNA polymerase II. *Nat Rev Mol Cell Biol* **16**, 167-77 (2015).
11. Brown, S.A., Imbalzano, A.N. & Kingston, R.E. Activator-dependent regulation of transcriptional pausing on nucleosomal templates. *Genes Dev* **10**, 1479-90 (1996).
12. Zobeck, K.L., Buckley, M.S., Zipfel, W.R. & Lis, J.T. Recruitment timing and dynamics of transcription factors at the Hsp70 loci in living cells. *Mol Cell* **40**, 965-75 (2010).
13. Bunch, H. HSF1 in RNA Polymerase II Promoter-Proximal Pausing and HSP70 Transcription. in *Heat Shock Proteins in Inflammatory Diseases* (eds. Asea, A.A.A. & Kaur, P.) 489-508 (Springer International Publishing, Cham, 2021).
14. Scheidegger, A. et al. Genome-wide RNA pol II initiation and pausing in neural progenitors of the rat. *BMC Genomics* **20**, 477 (2019).
15. Gorbovytska, V. et al. Enhancer RNAs stimulate Pol II pause release by harnessing multivalent interactions to NELF. *Nat Commun* **13**, 2429 (2022).
16. Petrenko, N. & Struhl, K. Comparison of transcriptional initiation by RNA polymerase II across eukaryotic species. *Elife* **10**(2021).
17. Yang, Y. et al. HIF-1 Interacts with TRIM28 and DNA-PK to release paused RNA polymerase II and activate target gene transcription in response to hypoxia. *Nat Commun* **13**, 316 (2022).

18. Galbraith, M.D. et al. HIF1A employs CDK8-mediator to stimulate RNAPII elongation in response to hypoxia. *Cell* **153**, 1327-39 (2013).
19. Core, L. & Adelman, K. Promoter-proximal pausing of RNA polymerase II: a nexus of gene regulation. *Genes Dev* **33**, 960-982 (2019).
20. Adelman, K. & Lis, J.T. Promoter-proximal pausing of RNA polymerase II: emerging roles in metazoans. *Nat Rev Genet* **13**, 720-31 (2012).
21. Vos, S.M., Farnung, L., Urlaub, H. & Cramer, P. Structure of paused transcription complex Pol II-DSIF-NELF. *Nature* **560**, 601-606 (2018).
22. Szlachta, K. et al. Alternative DNA secondary structure formation affects RNA polymerase II promoter-proximal pausing in human. *Genome Biol* **19**, 89 (2018).
23. Mines, R.C., Lipniacki, T. & Shen, X. Slow nucleosome dynamics set the transcriptional speed limit and induce RNA polymerase II traffic jams and bursts. *PLoS Comput Biol* **18**, e1009811 (2022).
24. Bunch, H. et al. TRIM28 regulates RNA polymerase II promoter-proximal pausing and pause release. *Nat Struct Mol Biol* **21**, 876-83 (2014).
25. Chen, F.X. et al. PAF1, a Molecular Regulator of Promoter-Proximal Pausing by RNA Polymerase II. *Cell* **162**, 1003-15 (2015).
26. Tettey, T.T. et al. A Role for FACT in RNA Polymerase II Promoter-Proximal Pausing. *Cell Rep* **27**, 3770-3779 e7 (2019).
27. Rahl, P.B. et al. c-Myc regulates transcriptional pause release. *Cell* **141**, 432-45 (2010).
28. Pommier, Y., Sun, Y., Huang, S.N. & Nitiss, J.L. Roles of eukaryotic topoisomerases in transcription, replication and genomic stability. *Nat Rev Mol Cell Biol* **17**, 703-721 (2016).
29. Puc, J. et al. Ligand-dependent enhancer activation regulated by topoisomerase-I activity. *Cell* **160**, 367-80 (2015).
30. Bunch, H. RNA polymerase II pausing and transcriptional regulation of the HSP70 expression. *Eur J Cell Biol* **96**, 739-745 (2017).
31. Yamamoto, T. et al. Continuous ERK activation downregulates antiproliferative genes throughout G1 phase to allow cell-cycle progression. *Curr Biol* **16**, 1171-82 (2006).
32. Hentze, N., Le Breton, L., Wiesner, J., Kempf, G. & Mayer, M.P. Molecular mechanism of thermosensory function of human heat shock transcription factor Hsf1. *Elife* **5**(2016).
33. Vihervaara, A. & Sistonen, L. HSF1 at a glance. *J Cell Sci* **127**, 261-6 (2014).
34. Gille, H. et al. ERK phosphorylation potentiates Elk-1-mediated ternary complex formation and transactivation. *EMBO J* **14**, 951-62 (1995).
35. Monje, P., Hernandez-Losa, J., Lyons, R.J., Castellone, M.D. & Gutkind, J.S. Regulation of the transcriptional activity of c-Fos by ERK. A novel role for the prolyl isomerase PIN1. *J Biol Chem* **280**, 35081-4 (2005).
36. Lis, J.T., Mason, P., Peng, J., Price, D.H. & Werner, J. P-TEFb kinase recruitment and function at heat shock loci. *Genes Dev* **14**, 792-803 (2000).
37. Ju, B.G. et al. A topoisomerase IIbeta-mediated dsDNA break required for regulated transcription. *Science* **312**, 1798-802 (2006).
38. McKinnon, P.J. Topoisomerases and the regulation of neural function. *Nat Rev Neurosci* **17**, 673-679 (2016).
39. Herrero-Ruiz, A. et al. Topoisomerase IIalpha represses transcription by enforcing promoter-proximal pausing. *Cell Rep* **35**, 108977 (2021).

40. Singh, S. et al. Pausing sites of RNA polymerase II on actively transcribed genes are enriched in DNA double-stranded breaks. *J Biol Chem* **295**, 3990-4000 (2020).
41. Sasanuma, H. et al. BRCA1 ensures genome integrity by eliminating estrogen-induced pathological topoisomerase II-DNA complexes. *Proc Natl Acad Sci U S A* **115**, E10642-E10651 (2018).
42. Shi, Q. et al. Estradiol increases risk of topoisomerase IIbeta-mediated DNA strand breaks to initiate Xp11.2 translocation renal cell carcinoma. *Cell Commun Signal* **19**, 114 (2021).
43. Wu, H.Y., Shyy, S.H., Wang, J.C. & Liu, L.F. Transcription generates positively and negatively supercoiled domains in the template. *Cell* **53**, 433-40 (1988).
44. Ma, J., Bai, L. & Wang, M.D. Transcription under torsion. *Science* **340**, 1580-3 (2013).
45. Wang, J.C. Cellular roles of DNA topoisomerases: a molecular perspective. *Nat Rev Mol Cell Biol* **3**, 430-40 (2002).
46. Nitiss, J.L. DNA topoisomerase II and its growing repertoire of biological functions. *Nat Rev Cancer* **9**, 327-37 (2009).
47. McKie, S.J., Neuman, K.C. & Maxwell, A. DNA topoisomerases: Advances in understanding of cellular roles and multi-protein complexes via structure-function analysis. *Bioessays* **43**, e2000286 (2021).
48. Carpenter, A.J. & Porter, A.C. Construction, characterization, and complementation of a conditional-lethal DNA topoisomerase IIalpha mutant human cell line. *Mol Biol Cell* **15**, 5700-11 (2004).
49. Austin, C.A. et al. TOP2B: The First Thirty Years. *Int J Mol Sci* **19**(2018).
50. Nitiss, J.L. Targeting DNA topoisomerase II in cancer chemotherapy. *Nat Rev Cancer* **9**, 338-50 (2009).
51. Dickey, J.S. & Osheroff, N. Impact of the C-terminal domain of topoisomerase IIalpha on the DNA cleavage activity of the human enzyme. *Biochemistry* **44**, 11546-54 (2005).
52. Vanden Broeck, A. et al. Structural basis for allosteric regulation of Human Topoisomerase IIalpha. *Nat Commun* **12**, 2962 (2021).
53. Chen, S.F. et al. Structural insights into the gating of DNA passage by the topoisomerase II DNA-gate. *Nat Commun* **9**, 3085 (2018).
54. Wu, C.C. et al. Structural basis of type II topoisomerase inhibition by the anticancer drug etoposide. *Science* **333**, 459-62 (2011).
55. Selvaraj, A. & Prywes, R. Expression profiling of serum inducible genes identifies a subset of SRF target genes that are MKL dependent. *BMC Mol Biol* **5**, 13 (2004).
56. Iyer, V.R. et al. The transcriptional program in the response of human fibroblasts to serum. *Science* **283**, 83-7 (1999).
57. Zhang, W. & Liu, H.T. MAPK signal pathways in the regulation of cell proliferation in mammalian cells. *Cell Res* **12**, 9-18 (2002).
58. Vantaggiato, C. et al. ERK1 and ERK2 mitogen-activated protein kinases affect Ras-dependent cell signaling differentially. *J Biol* **5**, 14 (2006).
59. Busca, R., Pouyssegur, J. & Lenormand, P. ERK1 and ERK2 Map Kinases: Specific Roles or Functional Redundancy? *Front Cell Dev Biol* **4**, 53 (2016).
60. Gagliardi, M. et al. Differential functions of ERK1 and ERK2 in lung metastasis processes in triple-negative breast cancer. *Sci Rep* **10**, 8537 (2020).
61. Satoh, Y. et al. Extracellular signal-regulated kinase 2 (ERK2) knockdown mice show deficits in long-term memory; ERK2 has a specific function in learning and memory. *J Neurosci* **27**, 10765-76 (2007).
62. Fremin, C., Saba-El-Leil, M.K., Levesque, K., Ang, S.L. & Meloche, S. Functional Redundancy of ERK1 and ERK2 MAP Kinases during Development. *Cell Rep* **12**, 913-21 (2015).

63. Shapiro, P.S. et al. Extracellular signal-regulated kinase activates topoisomerase IIalpha through a mechanism independent of phosphorylation. *Mol Cell Biol* **19**, 3551-60 (1999).
64. Bunch, H. et al. RNA polymerase II promoter-proximal pausing in mammalian long non-coding genes. *Genomics* **108**, 64-77 (2016).
65. Smorodinsky-Atias, K. et al. Intrinsically active variants of Erk oncogenically transform cells and disclose unexpected autophosphorylation capability that is independent of TEY phosphorylation. *Mol Biol Cell* **27**, 1026-39 (2016).
66. Schellenberg, M.J., Petrovich, R.M., Malone, C.C. & Williams, R.S. Selectable high-yield recombinant protein production in human cells using a GFP/YFP nanobody affinity support. *Protein Sci* **27**, 1083-1092 (2018).
67. Zhang, K. Gctf: Real-time CTF determination and correction. *J Struct Biol* **193**, 1-12 (2016).
68. Kimanius, D., Forsberg, B.O., Scheres, S.H. & Lindahl, E. Accelerated cryo-EM structure determination with parallelisation using GPUs in RELION-2. *Elife* **5**(2016).
69. Tegunov, D. & Cramer, P. Real-time cryo-electron microscopy data preprocessing with Warp. *Nat Methods* **16**, 1146-1152 (2019).
70. Bepler, T. et al. Positive-unlabeled convolutional neural networks for particle picking in cryo-electron micrographs. *Nat Methods* **16**, 1153-1160 (2019).
71. Pettersen, E.F. et al. UCSF Chimera--a visualization system for exploratory research and analysis. *J Comput Chem* **25**, 1605-12 (2004).
72. Emsley, P., Lohkamp, B., Scott, W.G. & Cowtan, K. Features and development of Coot. *Acta Crystallogr D Biol Crystallogr* **66**, 486-501 (2010).
73. Adams, P.D. et al. PHENIX: a comprehensive Python-based system for macromolecular structure solution. *Acta Crystallogr D Biol Crystallogr* **66**, 213-21 (2010).
74. Chen, V.B. et al. MolProbity: all-atom structure validation for macromolecular crystallography. *Acta Crystallogr D Biol Crystallogr* **66**, 12-21 (2010).
75. Odrowaz, Z. & Sharrocks, A.D. ELK1 uses different DNA binding modes to regulate functionally distinct classes of target genes. *PLoS Genet* **8**, e1002694 (2012).
76. Brenan, L. et al. Phenotypic Characterization of a Comprehensive Set of MAPK1/ERK2 Missense Mutants. *Cell Rep* **17**, 1171-1183 (2016).
77. Jasek-Gajda, E., Jurkowska, H., Jasinska, M., Litwin, J.A. & Lis, G.J. Combination of ERK2 inhibitor VX-11e and voreloxin synergistically enhances anti-proliferative and pro-apoptotic effects in leukemia cells. *Apoptosis* **24**, 849-861 (2019).
78. Fremin, C. et al. ERK2 but not ERK1 plays a key role in hepatocyte replication: an RNAi-mediated ERK2 knockdown approach in wild-type and ERK1 null hepatocytes. *Hepatology* **45**, 1035-45 (2007).
79. Alter, B.J., Zhao, C., Karim, F., Landreth, G.E. & Gereau, R.W.t. Genetic targeting of ERK1 suggests a predominant role for ERK2 in murine pain models. *J Neurosci* **30**, 11537-47 (2010).
80. Marchi, M. et al. The N-terminal domain of ERK1 accounts for the functional differences with ERK2. *PLoS One* **3**, e3873 (2008).
81. Eblen, S.T., Catling, A.D., Assanah, M.C. & Weber, M.J. Biochemical and biological functions of the N-terminal, noncatalytic domain of extracellular signal-regulated kinase 2. *Mol Cell Biol* **21**, 249-59 (2001).
82. Kolb, R.H., Greer, P.M., Cao, P.T., Cowan, K.H. & Yan, Y. ERK1/2 signaling plays an important role in topoisomerase II poison-induced G2/M checkpoint activation. *PLoS One* **7**, e50281 (2012).
83. Huang, K.C. et al. Topoisomerase II poisoning by ICRF-193. *J Biol Chem* **276**, 44488-94 (2001).

84. Xiao, H. et al. The topoisomerase IIbeta circular clamp arrests transcription and signals a 26S proteasome pathway. *Proc Natl Acad Sci U S A* **100**, 3239-44 (2003).
85. Kim, Y., Geiger, J.H., Hahn, S. & Sigler, P.B. Crystal structure of a yeast TBP/TATA-box complex. *Nature* **365**, 512-20 (1993).
86. Parekh, B.S. & Hatfield, G.W. Transcriptional activation by protein-induced DNA bending: evidence for a DNA structural transmission model. *Proc Natl Acad Sci U S A* **93**, 1173-7 (1996).
87. Kerppola, T.K. & Curran, T. The transcription activation domains of Fos and Jun induce DNA bending through electrostatic interactions. *EMBO J* **16**, 2907-16 (1997).
88. Acton, T.B., Mead, J., Steiner, A.M. & Vershon, A.K. Scanning mutagenesis of Mcm1: residues required for DNA binding, DNA bending, and transcriptional activation by a MADS-box protein. *Mol Cell Biol* **20**, 1-11 (2000).
89. McNamara, R.P. et al. KAP1 Recruitment of the 7SK snRNP Complex to Promoters Enables Transcription Elongation by RNA Polymerase II. *Mol Cell* **61**, 39-53 (2016).
90. Kahli, M., Osmundson, J.S., Yeung, R. & Smith, D.J. Processing of eukaryotic Okazaki fragments by redundant nucleases can be uncoupled from ongoing DNA replication in vivo. *Nucleic Acids Res* **47**, 1814-1822 (2019).
91. Cromie, G.A., Connelly, J.C. & Leach, D.R. Recombination at double-strand breaks and DNA ends: conserved mechanisms from phage to humans. *Mol Cell* **8**, 1163-74 (2001).
92. Michelini, F. et al. Damage-induced lncRNAs control the DNA damage response through interaction with DDRNAs at individual double-strand breaks. *Nat Cell Biol* **19**, 1400-1411 (2017).

Figures

Fig. 1.

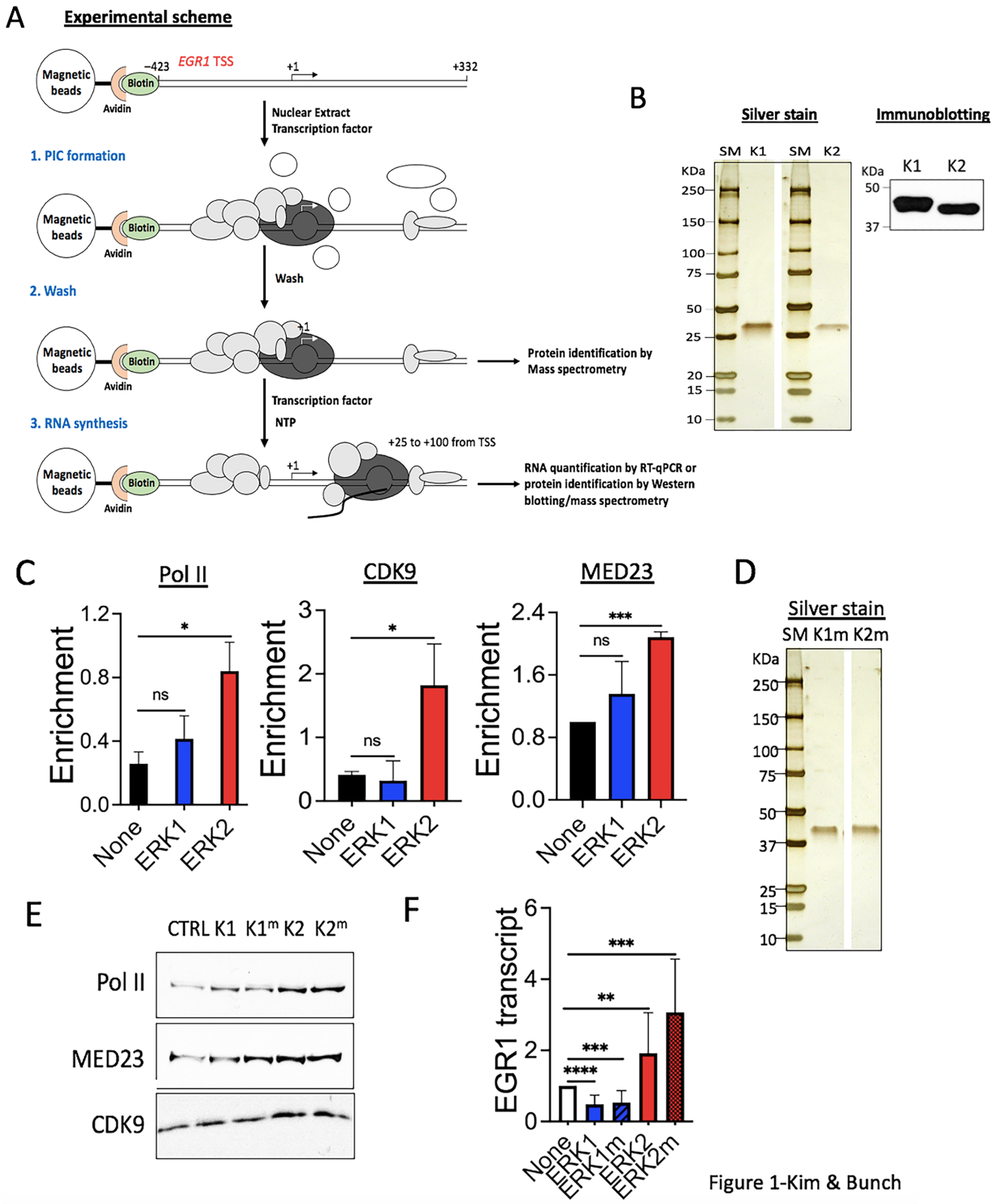

Figure 1-Kim & Bunch

Fig. 2.

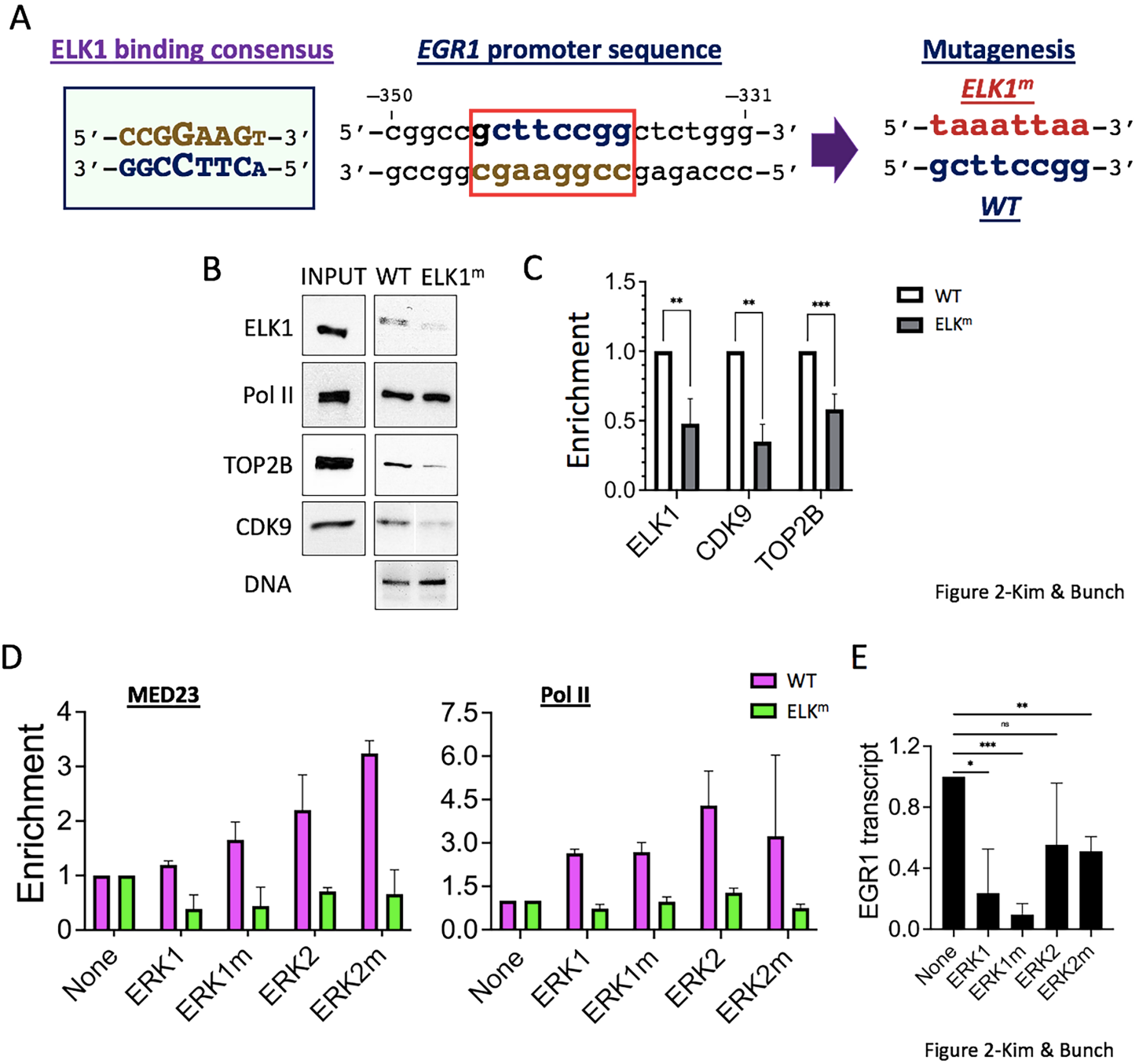

Fig. 3.

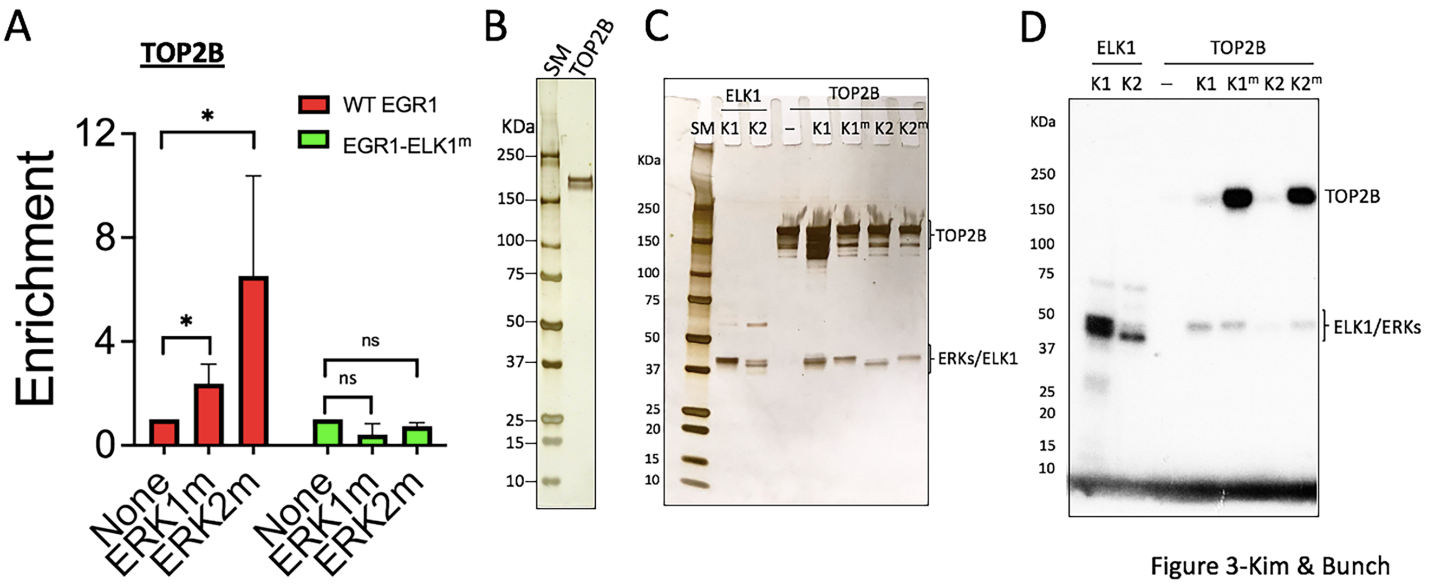

Figure 3-Kim & Bunch

Figure 3-Kim & Bunch

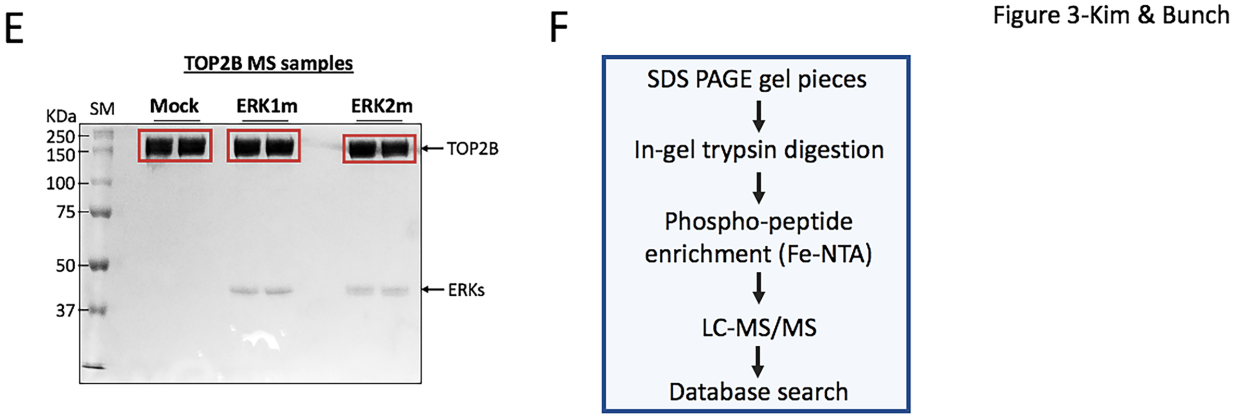

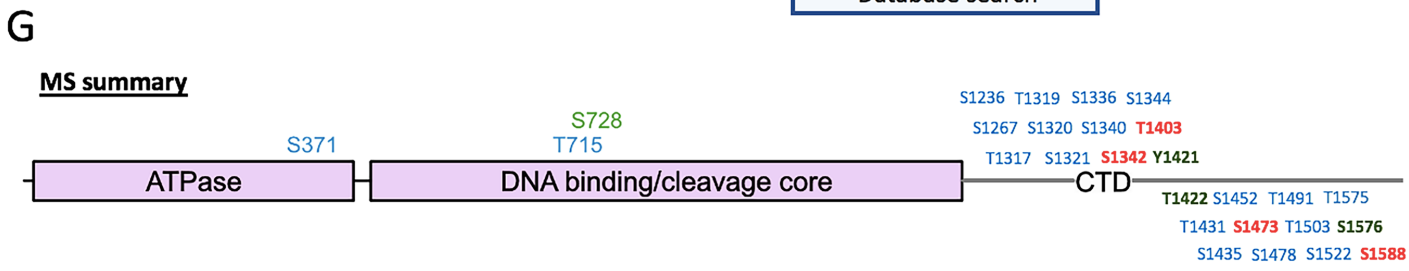

Fig. 4.

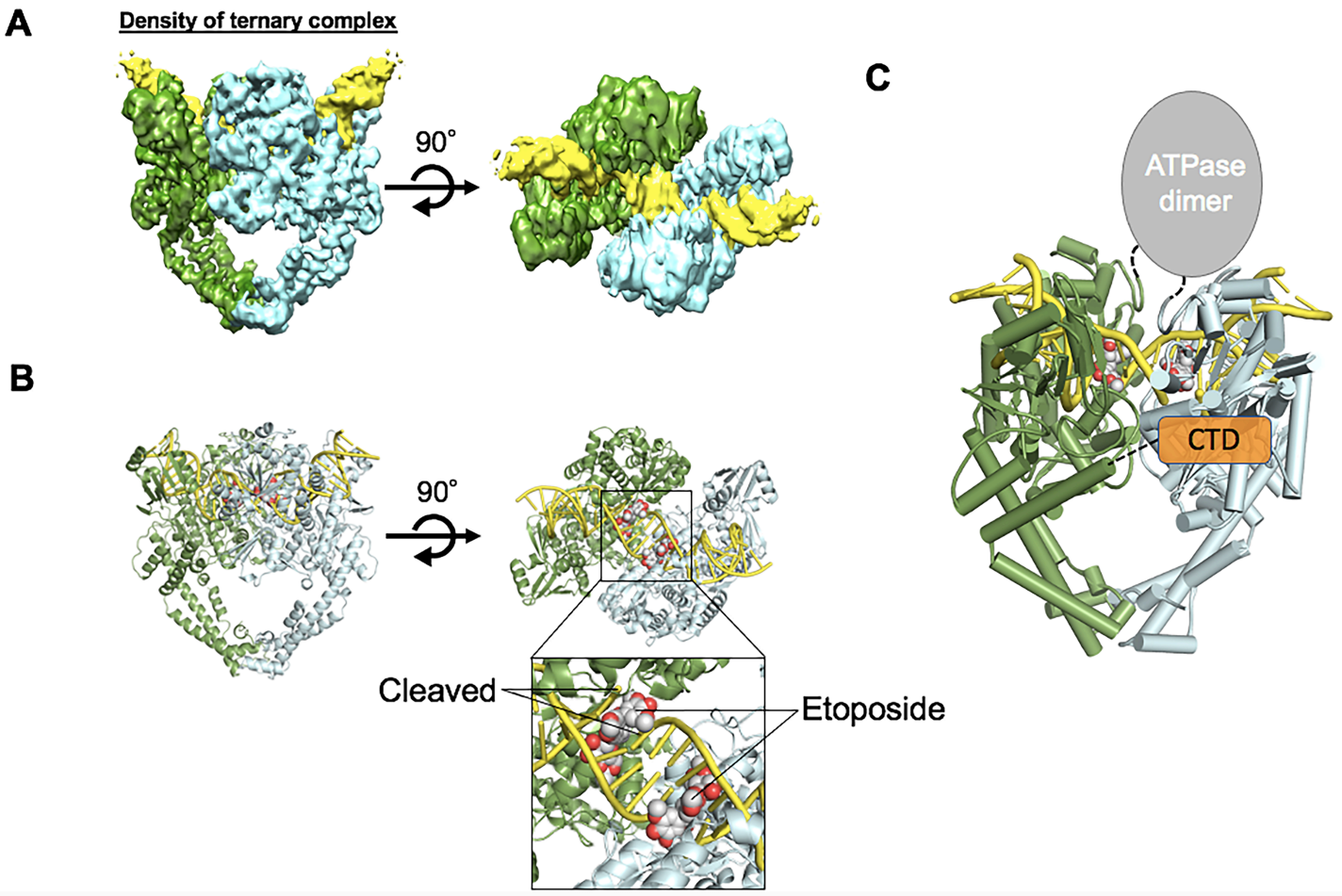

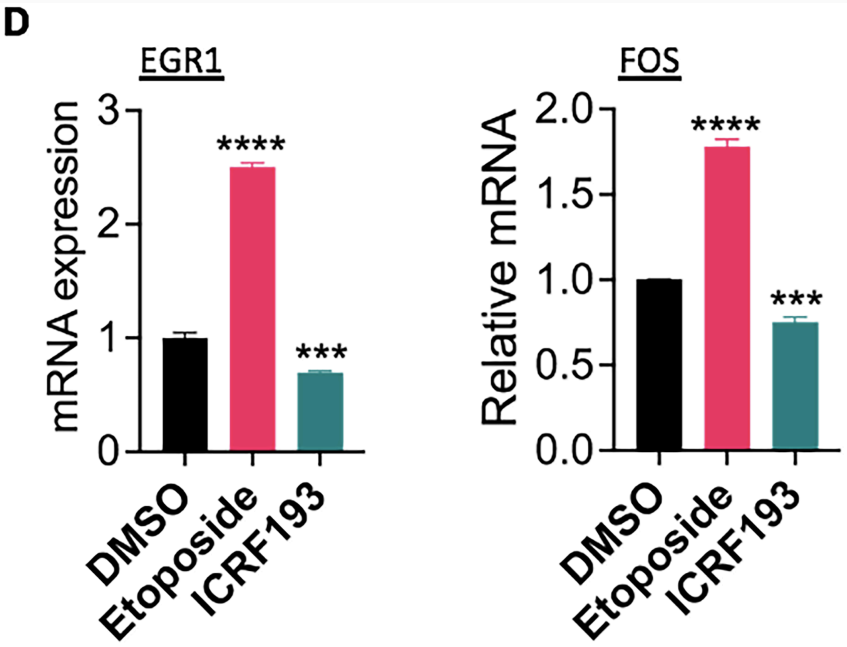

Figure 4-Kim & Bunch

Fig. 5.

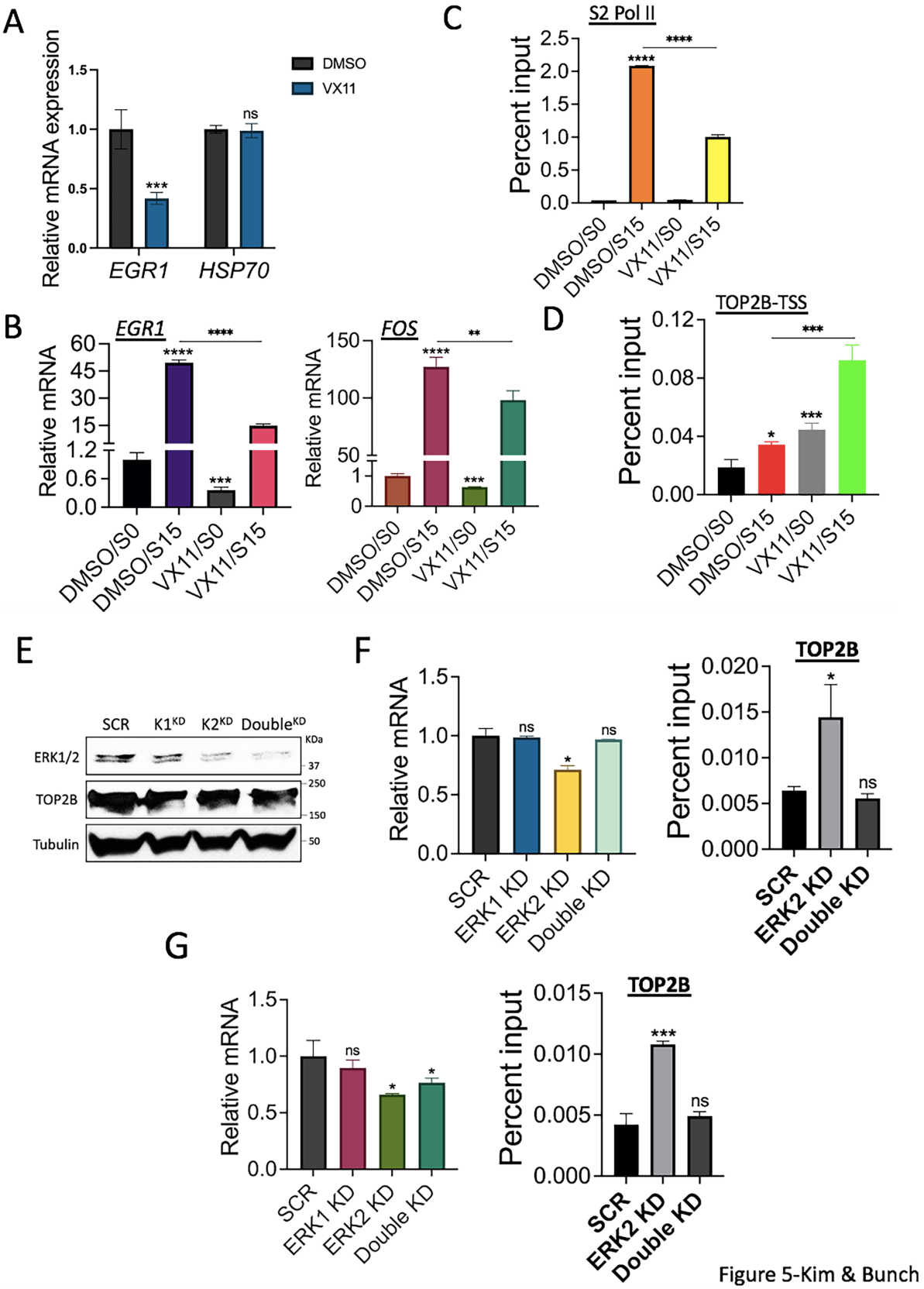

Figure 5-Kim & Bunch

Figure Legends

Fig. 1. ERK2, not ERK1, activates EGR1 transcription.

(**A**) A schematic representation of *in vitro* biochemical analyses used in this study. Grey and white circles without labels, proteins; a black curved line, a nascent RNA molecule.

(**B**) Left, silver-stained recombinant ERK1 (K1) and ERK2 (K2) proteins used in *in vitro* analyses. SM, standard protein size marker. Right, the result of immunoblotting confirming ERK1 and ERK2.

(**C**) Immobilized template assay results showing the increased occupancies of Pol II, CDK9, and MED23 by ERK2 on the *EGR1* TSS. Error bars, standard deviation throughout the figures. *P < 0.05, ***P < 0.005, not significant (ns).

(**D**) SDS-PAGE and silver-staining of the constitutively active ERK1m and ERK2m proteins.

(**E**) Immobilized template assay results of Pol II, CDK9, and MED23.

(**F**) *in vitro* transcription assay results showing *EGR1* gene activation by ERK2 and ERK2m. **P < 0.01, ***P < 0.005, ****P < 0.0005.

Fig. 2. ERK2-mediated transcriptional activation requires ELK1 binding to the *EGR1* promoter.

(**A**) ELK1 consensus sequence (left), a potential ELK1 binding site in the *EGR1* promoter, boxed in red (middle), and the mutation introduced to generate the ELK1^{m} template in this study (right).

(**B**) Immobilized template assay results showing decreased levels of ELK1, TOP2B, and CDK9 proteins on the ELK1^{m} template. INPUT, 25% of HeLa NE used for a reaction; DNA, the WT and ELK1^{m} immobilized template used for the assays.

(**C**) Statistical representation of immobilized template assay results. **P < 0.01, ***P < 0.005.

(**D**) Immobilized template assay results showing the effects of WT and mutant ERKs on MED23 and Pol II recruitment to the WT and ELK1^{m} template.

(**E**) *in vitro* transcription assay results showing *EGR1* gene suppression on the ELK1^{m} template. *P < 0.05, **P < 0.01, ***P < 0.005.

Fig. 3. TOP2B is phosphorylated by ERK1 and ERK2 proteins.

(**A**) Immobilized template assay results presenting TOP2B enrichment by ERK1m and ERK2 on the WT template but not on the ELK1^{m} template.

(**B**) Deubiquitinated TOP2B used for the *in vitro* kinase assays, silver-stained.

(**C**) Silver-stained reactions following the *in vitro* kinase assay.

(**D**) Autoradiograms of the *in vitro* kinase assay with TOP2B and ERKs. ELK1, a positive control.

(**E**) *In vitro* kinase assay followed by SDS-PAGE for the preparation of mass spectrometry analyses. Red boxes showing sliced gel pieces used for the analyses. MS, mass spectrometry.

(**F**) A flow chart showing the steps of mass spectrometry analyses performed in this study.

(**G**) A schematic representation of the TOP2B residues phosphorylated by ERK1m (green), ERK2m (red), or both kinases (blue).

Fig. 4. Cryo-EM structure of the ternary complex of TOP2B-etoposide-*EGR1* TSS.

(**A**) Density maps of the ternary complex in three different angles. Two TOP2B proteins shown in green and cyan, *EGR1* TSS in yellow.

(**B**) The ternary structure in ribbons. The DNA cleavage and etoposide binding sites, marked in a black box, are shown in close-up views. Two etoposide molecules are shown in sphere models, with the carbon and oxygen atoms colored white and red, respectively.

(**C**) Schematic representation of the entire TOP2B protein.

(**D**) qRT-PCR results indicating transcriptional activation and repression at the *EGR1* and *FOS* genes in the HEK293 cells treated with etoposide and ICRF193, respectively. ***P < 0.005, ****P < 0.0005.

Fig. 5. ERK2 function is required for normal TOP2B behavior and transcriptional activation.

(**A**) qRT-PCR results presenting the effects of ERK2 catalytic inhibition on *EGR1* and *HSP70* transcription. HEK293 cells were not synchronized. ***P < 0.005.

(**B**) qRT-PCR results presenting the effects of ERK2 catalytic inhibition on the *EGR*1 and *FOS* transcription. HEK293 cells were synchronized at G_0 (S0) before they were serum-induced to early G_1 (S15). **P < 0.01, ***P < 0.005, ****P < 0.0005.

(**C**) ChIP-qPCR results showing S2 Pol II occupancy changes in the *EGR1* gene with or without functional ERK2. ****P < 0.0005.

(**D**) ChIP-qPCR results showing a dramatic increase of TOP2B at *EGR1* upon the catalytic inhibition of ERK2. *P < 0.05, ***P < 0.005, ****P < 0.0005.

(**E**) Immunoblots of ERK1 ($K1^{KD}$), ERK2 ($K2^{KD}$), and ERK1/ERK2 double KD ($Double^{KD}$) HEK293 cells. Tubulin, a reference.

(**F**) qRT-PCR and ChIP-qPCR results presenting the effects of ERK KDs on *EGR1* transcription (left) and TOP2B occupancies at the *EGR1* TSS (right), respectively. *P < 0.05.

(**G**) qRT-PCR and ChIP-qPCR results presenting the effects of ERK KDs on *FOS* transcription (left) and TOP2B occupancies at the *FOS* TSS (right), respectively. *P < 0.05, ***P < 0.005.